Photoelectrochemical and Impedance Spectroscopic Investigation of Water Oxidation with "Co-Pi" coated Hematite Electrodes

Benjamin Klahr[†], Sixto Gimenez[‡], Francisco Fabregat-Santiago[‡], Juan Bisquert[‡], Thomas Hamann[†]*

[†] Department of Chemistry, Michigan State University, East Lansing, MI 48824-1322

[‡] Photovoltaics and Optoelectronic Devices Group, Departament de Física, Universitat Jaume I, 12071 Castelló, Spain

*Email: hamann@chemistry.msu.edu

Abstract

Uniform thin films of hematite (α-Fe_2O_3) deposited by atomic layer deposition (ALD) were coated with varying amounts of the cobalt phosphate catalyst, "Co-Pi." Steady state and transient photoelectrochemical studies were paired with impedance spectroscopic analysis in order to clarify the mechanism by which Co-Pi enhances the performance of hematite electrodes. It was found that under illumination, the Co-Pi catalyst can efficiently collect and store photogenerated holes from the hematite electrode. The improved charge separation reduces recombination which results in improved water oxidation performance.

Published as

Klahr, B.; Gimenez, S.; Fabregat-Santiago, F.; Bisquert, J.; Hamann, T. W. Photoelectrochemical and Impedance Spectroscopic Investigation of Water Oxidation with Co-Pi -Coated Hematite Electrodes, *Journal of the American Chemical Society* **2012**, *134*, 16693-16700.
Doi: 10.1021/ja306427f

Introduction

An increasing global energy demand combined with an increasing awareness of anthropogenic climate change has fueled the search for abundant and clean energy sources.[1] The sun illuminates the earth with abundant energy daily, where harvesting only a small fraction has the potential of satisfying the world's increasing energy demands in a carbon neutral fashion.[2] However, because this energy source is periodic for a given location, while our energy demands are not, an efficient method must be developed to store solar energy. One attractive strategy to storing solar energy is through photoelectrochemical (PEC) water splitting which stores energy in the bonds of H_2 and O_2. This concept was demonstrated in 1972 by Fujishima and Honda, yet no single material contains all of the necessary requirements in terms of stability, cost and efficiency.[3]

Hematite (α-Fe_2O_3) is one promising candidate for the water oxidation half reaction of PEC water splitting due to its adequate absorption of visible light less than 590 nm, suitably positive valence band capable of oxidizing water, and high stability under water oxidation conditions.[4-6] Also, iron oxide is nontoxic and abundant which makes it a practical material for large scale applications. Yet, a low charge collection length compared to a relatively large light penetration depth has historically limited efficient charge separation. This limitation is inherent to the chemical structure of hematite which is attributed to the minority charge mobility mechanism best described by small polaron hopping.[7,8] Despite this characteristic limitation, recent advances in nanostructuring, which orthogonalize light absorption and charge collection, has partially overcome this limitation and spurred renewed interest in this material.[9-12]

Another problem preventing efficient PEC water oxidation at hematite electrodes is the requirement of a large applied potential needed to produce a photocurrent. This large photocurrent onset potential is generally attributed to water oxidation kinetics at the hematite surface which competes with surface state recombination.[13-17] In order to reduce the required applied potential, various catalysts have been added to the hematite surface including IrO_2, Co ions and the cobalt phosphate catalyst, "Co-Pi".[18-24] Co-Pi has specifically gained a lot of recent attention because it uses earth-abundant elements, shows effective water oxidation characteristics and is stable over time due to its "self-healing" mechanism.[25-27] Consequently, it has also been applied to many potential photoanodes including ZnO, $BiVO_4$, Si and Fe_2O_3, and has shown improvements in both current onset potential and photocurrent density.[19-23,28-33] The reasons for this improvement, however, are not yet fully understood. Thus far, increased

performance has been attributed to increasing oxygen evolution kinetics,[19] increasing band bending and facilitating charge separation.[19,20,23] Despite the cathodic shift frequently measured for Co-Pi coated electrodes, Co-Pi it is not a perfect catalyst. This has been pointed out by Zhong and Gamelin who described evidence of a kinetic bottleneck on Co-Pi coated hematite electrodes.[21] The physical origin of both the improvement and the limits of water oxidation at Co-Pi coated hematite electrodes should be accurately understood so that better catalysts and strategies for improvement can be designed.

In this work, we employ photoelectrochemical measurements and impedance spectroscopy to investigate the effect of the Co-Pi catalyst on thin film hematite electrodes. The thin film hematite was prepared by atomic layer deposition (ALD),[34-36] and were subsequently coated with Co-Pi films by photoelectrodeposition. These thin hematite films have been shown to be a good model system for studying the limitations of water oxidation at the hematite surface.[37,38] Also, the planar geometry of these films allowed us to perform a controlled thickness dependence where increasing the amount of Co-Pi deposited uniformly increases the Co-Pi thickness in one dimension. Co-Pi coated hematite film were then analyzed by impedance spectroscopy and PEC experiments as a function of Co-Pi thickness to elucidate the factors controlling the enhanced performance of the Co-Pi coated hematite electrode.

Experimental

Thin films of hematite were deposited on fluorine-doped tin oxide (FTO) coated glass substrates (Hartford Glass, 12 Ωcm^{-2}) by ALD (Savannah 100, Cambridge Nanotech Inc.) using ferrocene as the metal precursor and ozone as the oxidation source. ALD is a process which employs alternating metal precursor and oxidation pulses each separated by a nitrogen purge such that chemistry only occurs in a self-limiting fashion where the previous precursor has adsorbed. The metal precursor was heated to 70 C and pulsed for 20 seconds. After purging the oxidation pulse was performed. The oxidation pulse consisted of a 0.015 second pulse of H_2O, immediately followed by a 1 second pulse of ozone (~4.5% by weight O_3 in O_2 produced by Yanco Industries ozone generator), followed by a 5 second purge time. This cycle was performed 10 times to create 1 oxidation macrocycle. Integrating water with O_3 as an oxidation source has been shown to increase the growth rate and uniformity of In_2O_3 films deposited by ALD.[39] Films were prepared by 1,000 ALD cycles and measured to be ~55 nm by absorption measurements (Perkin Elmer, Lambda 35 with a Labsphere integrating sphere) corrected for reflection as described previously, as well as ellipsometric measurements (Horiba Jobin Yvon, Smart-SE).[36] Films were characterized by Raman Spectroscopy and XRD of these films previously.[36] Hematite electrodes were masked with a 60 μm Surlyn film (Solaronix) with a 0.28 cm^2 hole to define the active area and to

prevent scratching of the thin films. Surlyn films were adhered to the electrodes by heating to 120° C. The protected hematite films were clamped to a custom made glass electrochemical cell. A homemade saturated Ag/AgCl electrode was used as a reference electrode and high surface area platinum mesh was used as the counter electrode.

Co-Pi catalyst films were deposited by photoelectrodeposion which was originally described on ZnO electrode by Steinmiller and Choi and later adapted to hematite by Zhong and Gamelin.[22,33] Photoelectrodeposition has been shown to provide a superior deposition at the photoactive anode which is in contrast to electrodeposition which favors deposition at the underlying conductive substrate.[21,22,33] Hematite electrodes were immersed in a solution containing 0.5 mM $Co(NO_3)_2 \cdot 6H_2O$ in a 0.1 M phosphate buffer (pH 6.9). A bias of 0.35 V vs Ag/AgCl was applied under illumination. At this potential, steady state water oxidation does not occur with or without the Co-Pi catalyst, thus any charge passed is assumed to be due to deposition of the catalyst. The Co-Pi films are flat and uniform as shown in an SEM image of a thick Co-Pi film deposited onto hematite in supporting information. The thickness of the Co-Pi layer was controlled by varying the amount of charge allowed to pass during the deposition. In this study, 5 thicknesses were prepared by allowing 1, 2, 15, 45 and 90 mC cm^{-2} to pass. Film thicknesses were measured to be ~ 2.5, 7.3, 12 and 55 nm by ellipsometry. Thicknesses were also estimated by assuming that a single electron passed deposits one cobalt atom with surrounding ligands which occupies 125$Å^3$.[25] The thicknesses of the Co-Pi layers deposited by 1, 2, 15, 45 and 90 mC cm^{-2} was calculated to be 8, 15, 113, 337 and 675 nm respectively, which agrees well with the ellipsometry measurements for all except the thickest layer of Co-Pi.

After the catalyst was deposited, the electrodes were lightly rinsed with DI water to remove any excess cobalt ions. The water oxidation properties of the catalyst coated hematite films were then examined in contact with an aqueous solution buffered at pH 6.9 using a 0.1 M phosophate buffer containing 200 mM KCl as a supporting electrolyte. The pH was determined with Fisher Scientific Accumet pH meter. Impedance spectroscopic and photoelectrochemical measurements were made with an Eco Chemie Autolab potentiostat coupled with Nova electrochemical software. Impedance data were gathered using a 10 mV amplitude perturbation of between 10,000 and 0.01 Hz. Data were fit using Zview software (Scribner Associates). The light source was a 450 W Xe arc lamp. An AM 1.5 solar filter was used to simulate sunlight at 100 mW cm^{-2}. All photoelectrochemical measurements were performed by shining light from the substrate-electrode (SE) interface which avoids competitive light absorption of the Co-Pi.

Light chopping *J-V* curves were measured at a rate of 75 mV/s. The light was chopped using a computer controlled ThorLabs solenoid shutter which was set to activate every 266 ms such that the light was turned on or off every 20 mV. Steady state *J-V* curves were measured at a scan rate of 5 mV/s.

Oxygen was detected by using an Ocean Optics spectrometer which probed the fluorescent decay of the FOSPOR patch. The FOSPOR patch was placed in solution which filled an airtight cell. The cell was filled so that very little headspace existed. The solution was stirred vigorously so that the O_2 measurement would be as close to real time as possible. Measurements were made under 4 sun illumination at 1.3 V vs RHE to increase oxygen production and reduce noise. In the calculation of the faradaic efficiency, the assumption was made that no oxygen diffused into the very small headspace during the timescale of these experiments.

While these experiments were performed multiple times with many electrodes, only 3 different, but nominally identical electrodes were used to collect the data shown here: one for current transient and JV curves, one for EIS measurements and one for O_2 measurements. The use of one electrode for each experiment allowed us to control for small differences of different bare electrodes. For experiments with varying amounts of Co-Pi, the Co-Pi was removed by applying a potential of 0 V vs Ag/AgCl under dark conditions which slowly removed the Co-Pi film. After the Co-Pi was removed, the electrodes were examined to ensure that the performance was consistent with a bare electrode before applying Co-Pi for the next experiment.

Results and Discussion

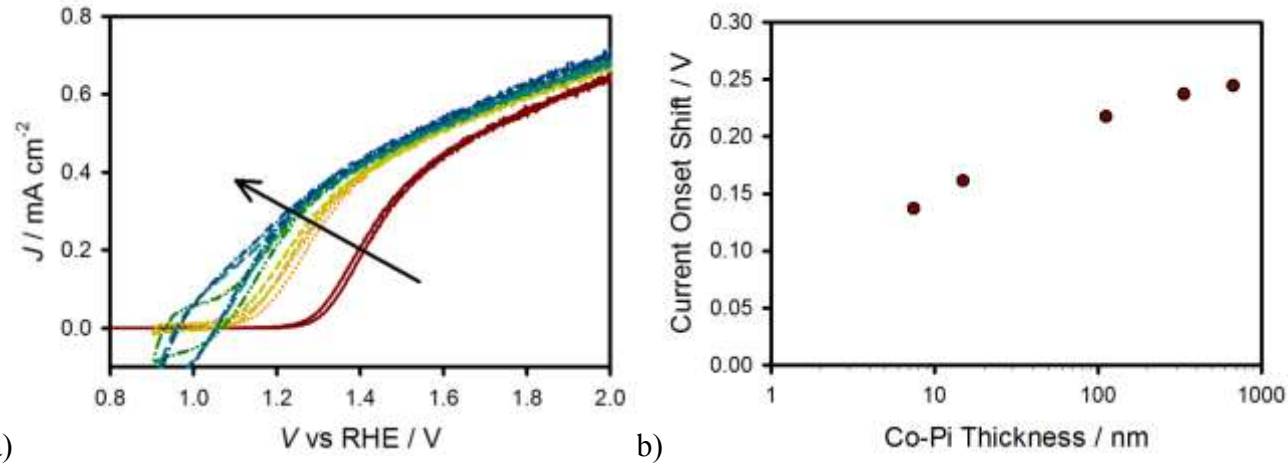

a) b)

Figure 1. a) *J-V* curves measured at 5 mV/s of a bare α-Fe_2O_3 electrode (red solid line) and the same electrode with 8 (orange dotted line) 15 (yellow short dashed line) 113 (green dashed double dotted line)

337 (teal long dashed line) and 675 (blue dashed single dotted line) nm Co-Pi catalyst in contact with a pH 6.9 buffered aqueous solution under 1 sun illumination. b) Potential shift of the current onset relative to the bare electrode measured at 200mA cm^{-2}.

Current density, *J*, vs. applied voltage, *V*, curves measured under 1 sun (100 mW cm^{-2}) illumination for a bare hematite electrode and the same hematite electrode coated with the varying thicknesses of the Co-Pi catalyst can be seen in figure 1a. Steady state current measurements were also performed where the photocurrent was sampled after stabilizing over several minutes at each individual potential (see supporting information). It was found that the steady state currents are equal to the currents of the cathodic scan of the *J-V* curves, thus confirming that the *J-V* measurements presented herein represent steady-state behavior. The faradaic efficiency of the *J-V* curves was also measured by a fluorescent O_2 sensor. The O_2 concentration was measured at 1.3 V vs RHE which showed an increase in detected O_2 with increasing Co-Pi thickness for Co-Pi thicknesses up to 113 nm, also consistent with the *J-V* curves. The O_2 detected was consistent with ~100% faradaic efficiency when considering the number of coulombs that have passed (supporting information). Figure 1b shows the cathodic shift the of the *J-V* curves in Fig 1a by sampling the potential needed to sustain a 200 μA cm^{-2} current density. The shift in photocurrent onset potential increases with Co-Pi thickness. This behavior is consistent with experiments examining Co-Pi on planar FTO coated glass, which was attributed to an increase in the number of active catalytic sites.[25] This trend, however, was not observed in a recent study examining Co-Pi deposited on high surface area hematite.[22] Thus, the simple explanation of increasing the number of active catalytic cites does not adequately describe the enhanced performance of the Co-Pi–hematite system. An alternative explanation is discussed below. In addition to the shift of the *J-V* curve, a slight increase in the photocurrent density at potentials positive of 1.4 V vs RHE is observed. This enhancement, however, is independent of Co-Pi thickness. The improved PEC performance is generally consistent with previous reports of Co-Pi coated hematite electrodes.[19,22,23]

While performing steady state measurements, it became apparent that increasing the Co-Pi thickness required an increasing amount of time to reach steady state. Current transients were measured in response to turning on (anodic) and off (cathodic) 1 sun illumination at a constant potential. Examples of anodic and cathodic current transients for different thicknesses of Co-Pi on hematite electrodes can be seen in figures 2a and 2b, respectively, at an applied potential of 1.1 V vs RHE. As shown previously for bare hematite electrodes, at potentials negative of the current onset potential (such

as 1.1 V vs RHE), an anodic spike in current is visible when the light is turned on which quickly decays to the steady state current density. When the light is turned off a cathodic spike in current is observed which quickly decays to J_0. These spikes have been attributed to the charging (trapping of holes) and discharging of surface states, or oxidizing and reducing surface species.[37] Analogous behavior is observed when Co-Pi is added to the surface of hematite, however the amount of charge passed in the transients obviously increases with Co-Pi thickness. Both the anodic and cathodic charging currents scale with Co-Pi thickness suggesting that the process governing the transients is governed by the Co-Pi and is reversible. The transient anodic current is attributed to the oxidation of Co(III) in the Co-Pi catalyst layer to Co(IV) by photogenerated holes in the valence band. This assignment is based on the recent observation of Co(IV) by EPR from Co-Pi which was electrodeposited during water oxidation.[40] This is also consistent with the fact that the charge passed in anodic transients decreases with increasing positive potentials where band bending increases and the concentration of electrons at the surface able to recombine decreases (supporting information). Since such a large amount of charge is passed, and the quantity scales with thickness of the Co-Pi layer, the catalyst film must have the Co(IV) species distributed throughout. This indicates efficient diffusion of holes in the catalyst film, via charge transfer from/to the cobalt centers consistent with recent self-exchange measurements of Co-Pi using a model cubane molecule.[41] The cathodic current measured after turning the light off is attributed to the reduction of the Co(IV) to Co(III) (recombination) by electrons from the conduction band of the hematite. This assignment of charge transfer to Co-Pi as a reversible process is consistent with mechanistic studies of Co-Pi on FTO through Tafel analysis.[25]

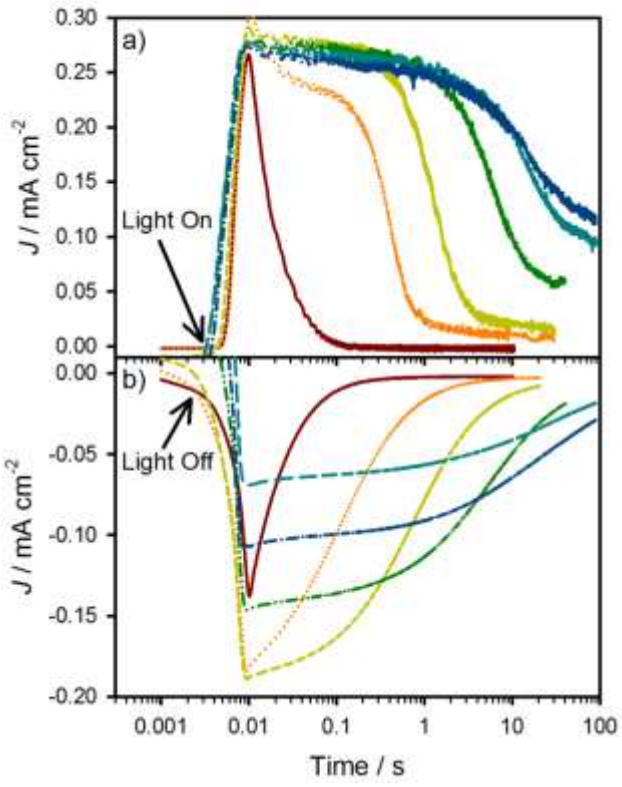

Figure 2. a) anodic and b) cathodic transients measured for a bare hematite electrode (red solid line) and the same electrode with 8 (orange dotted line) 15 (yellow short dashed line) 113 (green dashed double dotted line) 337 (teal long dashed line) and 675 (blue dashed single dotted line) nm Co-Pi catalyst in contact with a pH 6.9 buffered aqueous solution under 1 sun illumination at an applied bias of 1.1 V vs RHE.

Light chopping experiments were also performed for electrodes with varying thicknesses of Co-Pi. Figure 3 shows a *J-V* curve measured under chopped and constant 1 sun illumination for a 113 nm Co-Pi coated hematite electrode. This is compared to the *J-V* curve of the bare and Co-Pi coated electrode. The maximum current of the chopped light *J-V* is approximately linear which is reached instantaneously upon turning the light on. This behavior is similar to hematite electrodes measured in contact with an electrolyte containing a fast redox shuttle.[37,42,43] Two different regions are observed when comparing the chopped light *J-V* curve to the steady state *J-V* curve. One is at potentials positive of ~1.4 V vs RHE where the instantaneous photocurrent measured by chopped light is equal to the steady state *J-V* curve. The other region is between 0.9 and 1.4 V vs RHE where the instantaneous photocurrent measured by light chopping is much higher than the steady state photocurrent. In other

words, at these potentials, charge is being transferred to and stored in the Co-Pi without steady state water oxidation occurring. This "trapping" in the Co-Pi film presents an opportunity for recombination of electrons in the conduction band and Co(IV) to produce Co(III). Chopped light *J-V* curves measured for different Co-Pi thicknesses can be seen in supporting information.

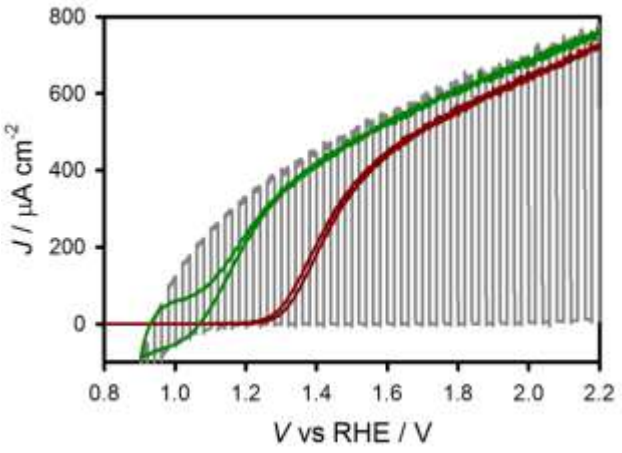

Figure 3. *J-V* curves measured under 1 sun illumination for a bare hematite (red line) and hematite coated with 113 nm Co-Pi (green line). Chopped illumination JV for Co-Pi coated electrode is also shown (grey line)

IS measurements were also performed for electrodes with varying thicknesses of Co-Pi. An example of a Nyquist plot measured for a bare hematite electrode and a hematite electrode coated with 113 nm of Co-Pi at 1.3 V vs RHE can be seen in figure 4. Around the photocurrent onset, two semicircles are clearly visible for both bare and Co-Pi coated hematite electrodes. The low frequency (high impedance) semicircle is clearly much smaller for Co-Pi coated electrodes compared to the bare electrodes. At more positive potentials (> 1.3 V vs RHE), the low frequency semicircle disappears for Co-Pi coated hematite electrodes.

The general equivalent circuit, EC, used to interpret the IS data is shown in figure 4a. The proposed EC includes the equivalent circuit established previously for a bare hematite electrode, which consists of the capacitance of the bulk hematite, C_{bulk}, charge transfer resistance from the valence band of the hematite, $R_{ct,bulk}$, a resistance which is related to the rate of trapping holes in surface states, R_{trap}, a capacitance of the surface states, C_{ss}, charge transfer from the surface states, $R_{ct,ss}$.[44] Additional electrical components were added to account for the Co-Pi layer; the capacitance of the Co-Pi layer, $C_{Co\text{-}Pi}$, and charge transfer resistance from the Co-Pi layer, $R_{ct,Co\text{-}Pi}$. Clearly, the full EC shown in figure 5a

cannot be used to unambiguously fit the IS data for Co-Pi coated. One thing that allowed us to simplify the equivalent circuit was independent examination of the low frequency semicircle; the capacitance of this feature increases approximately linearly with increasing Co-Pi thickness (shown and discussed below). This allowed assignment of this capacitance to $C_{Co\text{-}Pi}$, thus simplifying to the equivalent circuit to that shown in figure 5b.

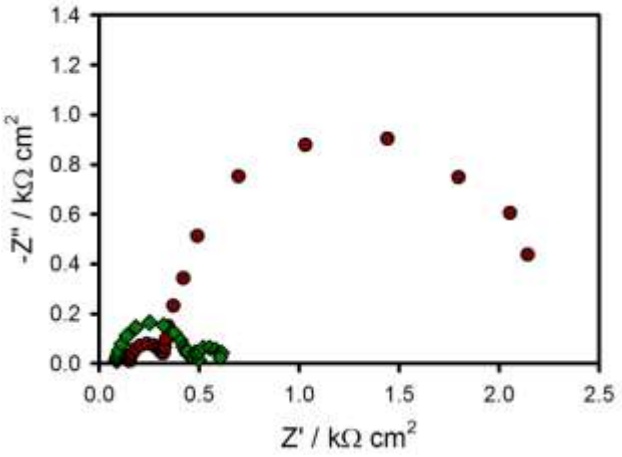

Figure 4. Nyquist plots of a bare hematite electrode (red circles) and with 113 nm Co-Pi catalyst (green triangles) measured at 1.3 V vs RHE.

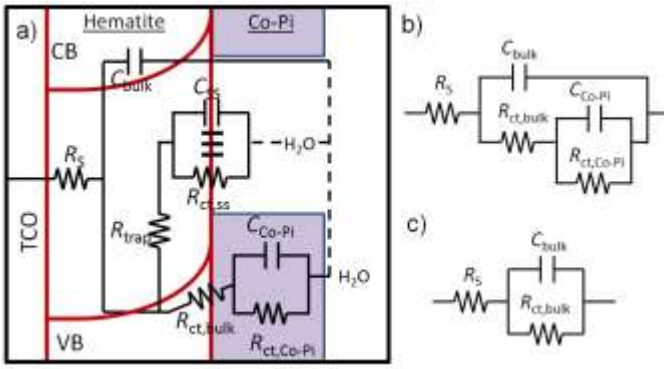

Figure 5. a) Proposed full equivalent circuit used for interpretation of Fe_2O_3 electrodes coated with Co-Pi catalyst. b) Simplified equivalent circuit used for interpretation of or Co-Pi coated Fe_2O_3. c) Randle's circuit used when only one semicircle is visible.

The impedance spectra of hematite electrodes with varying amounts of Co-Pi deposited were fit to the equivalent circuit shown in figure 5b. Figure 6a shows plots of $C_{Co\text{-}Pi}$ vs. applied potential for the different thicknesses of Co-Pi deposited on the hematite film. The $C_{Co\text{-}Pi}$ increases with thickness which

is consistent with the assignment of this capacitance to the chemical capacitance of Co-Pi. This is also consistent with the trend of increasing charge being passed before reaching a steady state current in the current transient measurements displayed in figure 2. The values for $R_{ct,Co\text{-}Pi}$, shown in figure 5b, are also related to the Co-Pi layer thickness; the resistance decreases with increasing Co-Pi thickness. When deposited on FTO, Co-Pi is known to be a porous material which shows a decrease in the required overpotential with an increasing amount of the catalyst.[25] The dependence of the decreasing $R_{ct,Co\text{-}Pi}$ with Co-Pi thickness is also consistent with the Co-Pi being a porous material. For all Co-Pi thicknesses, $R_{ct,Co\text{-}Pi}$ decreases exponentially with increasing potential. Similar to the current transients discussed above, there are 2 clear regions that are observed in the Nyquist plots. One is at potentials less than 1.4 V vs RHE which shows 2 clear semicircles where the contribution of the Co-Pi can be observed. However at potentials greater than 1.4 V vs RHE the low frequency capacitive feature disappears, and meaningful values for $C_{Co\text{-}Pi}$ and $R_{ct,Co\text{-}Pi}$ cannot be calculated. For these data, a simple Randle's circuit (figure 5c) is used to fit the impedance spectra and calculate values for $R_{ct,bulk}$ and C_{bulk}. The low frequency semicircle also disappears for bare hematite electrodes at more positive potentials (> 1.5 V vs RHE), which has recently been attributed a hole transfer from the surface states of iron oxide to solution which is not the rate limiting step of water oxidation at positive potentials.[38] Similarly, we propose that at potentials where this low frequency capacitive feature measured on Co-Pi coated electrodes disappear, charge transfer from the Co-Pi to solution is not the rate limiting step. This is the cause of the independence of photocurrent measured at potentials positive of ~1.4 V vs RHE for increasing Co-Pi thickness. At these positive potentials, the photocurrent is controlled by the number of holes that reach the hematite surface for both bare and Co-Pi coated hematite electrodes.[43]

Values of $R_{ct,bulk}$, which represent the charge transfer from the hematite to the Co-Pi catalyst, can be found in figure 6c. At potentials negative of where water oxidation begins (~0.8 – 1.2 V vs RHE), $R_{ct,bulk}$ is on the order of 10^2-10^3 Ω cm^2. These resistances are comparable to when a fast redox shuttle such as $[Fe(CN)_6]^{3-/4-}$ is used as a hole scavenger as reported previously.[37] This is consistent with having fast charge transfer of holes from the valence band of hematite to the Co-Pi. At potentials negative of the current onset potential, $R_{ct,Co\text{-}Pi}$ is much higher than $R_{ct,bulk}$. This is consistent with light chopping experiments where at these low applied potentials, charge transfer to Co-Pi is facile, however water oxidation from the Co-Pi does not occur according the steady state *J-V* curves and O_2 measurements. A plot showing $R_{ct,Co\text{-}Pi}$ and $R_{ct,bulk}$ in the same graph for comparison can be seen in supporting information which emphasizes which resistance is the limiting resistance for a given

potential. The total resistance, R_{tot} was calculated (R_s+ $R_{ct,Co\text{-}Pi}$ +$R_{ct,bulk}$) and compared to the resistance derived from the *J-V* curve ($R_{tot} = dV/dJ$). A plot of R_{tot} derived from both impedance and *J-V* results can be seen in supporting information. The overlap of the R_{tot} determined from IS and the *J-V* curve shows how $R_{ct,bulk}$ and $R_{ct,Co\text{-}Pi}$ determine the shape of the *J-V* curve.

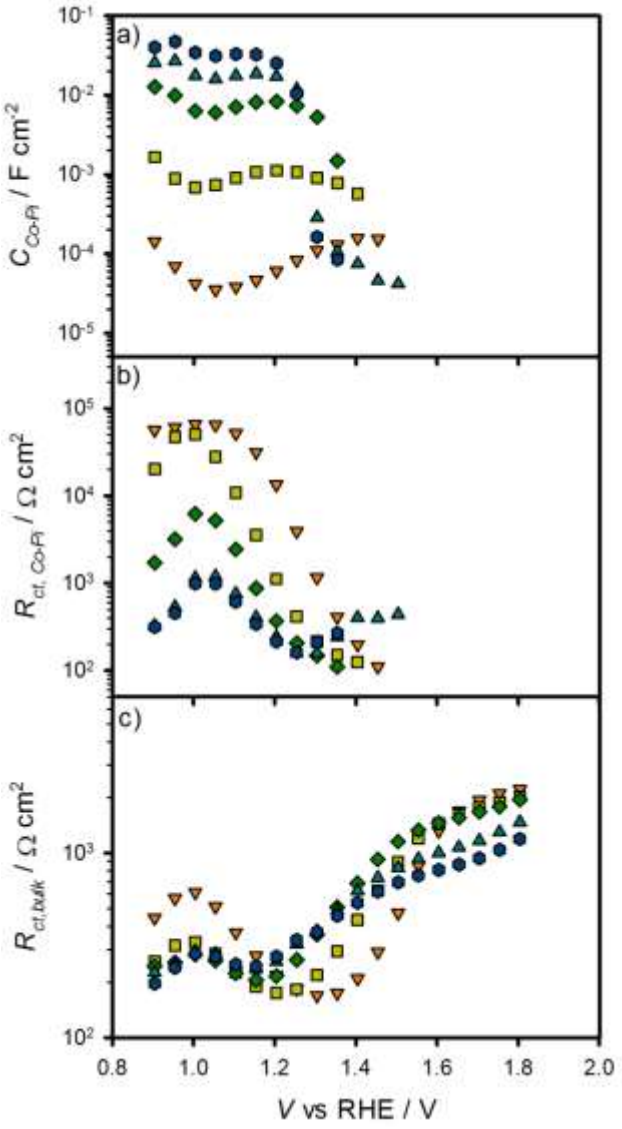

Figure 6. a) $C_{\text{Co-Pi}}$, b) $R_{ct,Co\text{-}Pi}$ and c) $R_{ct,bulk}$ values fit from impedance response of hematite electrodes with 8 (orange triangles pointing down), 15 (yellow squares), 113 (green diamonds) 337 (teal triangles pointing up) and 675 nm (blue hexagons).

Mott Schottky (MS) plots were prepared for Co-Pi coated hematite electrodes from C_{bulk} values determined from impedance spectroscopy which can be seen in figure 7. As shown previously for bare

hematite electrodes, a horizontal shift is observed under illumination which is attributed to Fermi level pinning. This Fermi level pinning is not observed in dark conditions. MS plots were also prepared for the same electrode with varying amounts of Co-Pi. The MS plots measured with the Co-Pi coated hematite electrode shows a much more linear MS compared to the bare electrode suggesting Fermi level pinning is reduced. Also, the flat band potential extrapolated from both bare and Co-Pi coated hematite electrodes is roughly the same suggesting that Co-Pi does not shift the bands. The MS plot measured in the dark for a Co-Pi coated hematite electrode also shows a shift toward higher bulk capacitances compared to the bare electrode (supporting information).

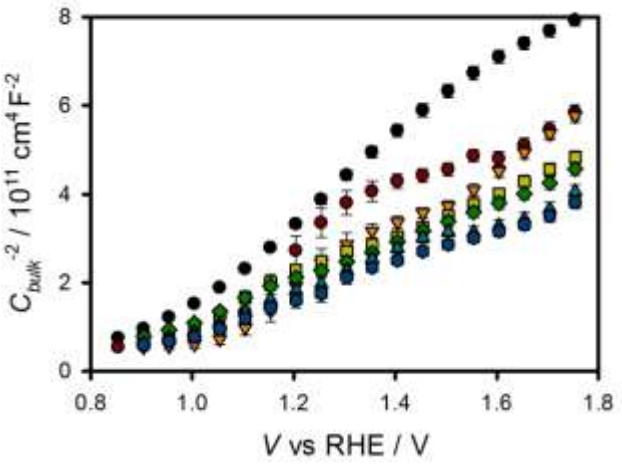

Figure 7. Mott Schottky plot prepared from C_{bulk} values determined by IS. Data includes bare hematite electrode measured under 1 sun illumination (red circles) and in the dark (black circles), as well as the same electrode coated with 8 (orange downward pointing triangles), 15 (yellow squares) 113 (green diamonds) 337 (teal upward pointing triangles) and 675 (blue hexagons) nm Co-Pi.

The PEC behavior of Co-Pi coated hematite electrodes was also examined as a function of incident light intensity. The *J-V* curves for a hematite electrode with 113 nm Co-Pi can be seen in figure 8 measured under 0.1, 0.33 and 1 sun illumination. There is a linear increase in photocurrent at positive potentials in addition to a shift in the current onset potential with increasing light intensity. This ideal behavior is consistent with the diode equation as discussed elsewhere.[45] IS measurements were also performed using the equivalent circuit in figure 5c to fit the impedance spectra. The resulting fits can be seen in figure 9. $C_{Co\text{-}Pi}$ has a slight increase with increasing light intensity and the peak shifts cathodically. This is analogous to the behavior of a surface state capacitance measured on hematite

electrodes as a function of light intensity.[38] The magnitude and shift of this capacitance confirms that it results from the Co-Pi and not from a Helmholtz capacitance. The $R_{ct,Co\text{-}Pi}$ shifts cathodically with light intensity which is consistent with the cathodic shift observed in the *J-V* curves. Also, a peak in $R_{ct,Co\text{-}Pi}$ shifts cathodic with increasing light intensity. $R_{ct,bulk}$ and C_{bulk} values can be found in supporting information.

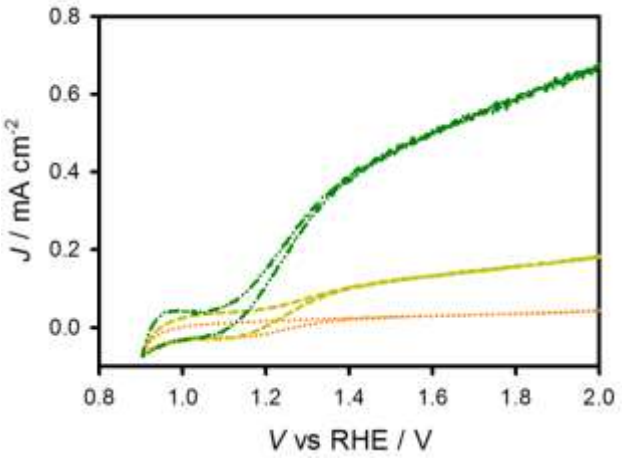

Figure 8. *J-V* curves of a hematite electrode coated with 113 nm Co-Pi under 0.1 (orange dotted line), 0.33 (yellow dashed line) and 1 sun illumination (green dashed dotted line).

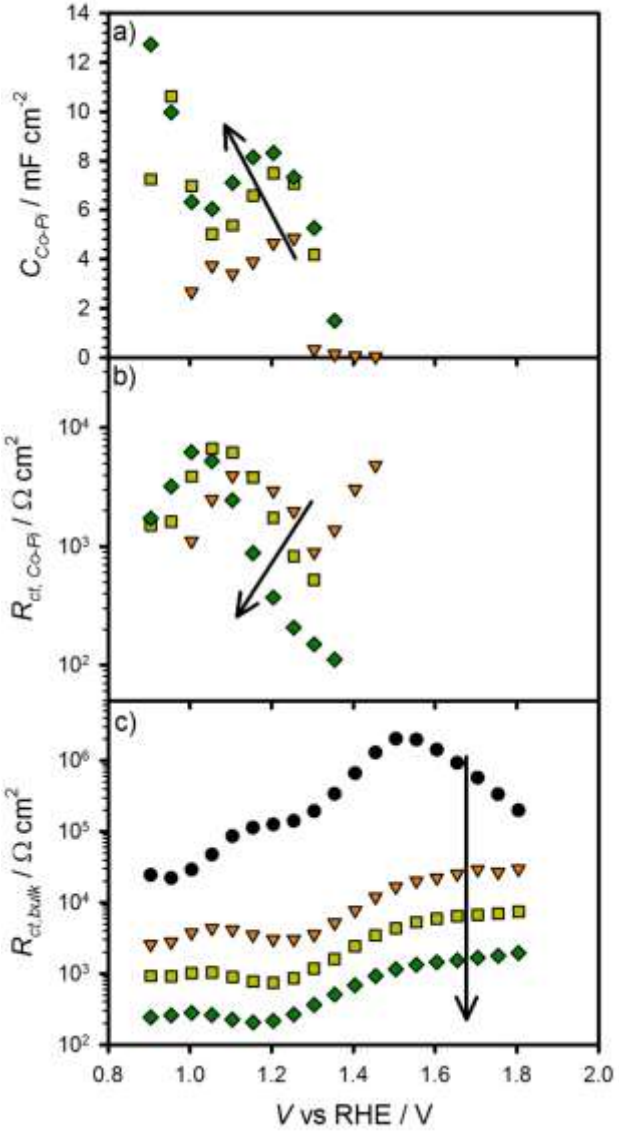

Figure 9. a) $C_{Co\text{-}Pi}$, b) $R_{ct,Co\text{-}Pi}$ and c) $R_{ct,bulk}$ fit from impedance spectra for a hematite electrode coated with 113 nm Co-Pi measured under 0.1 (orange dotted line), 0.33 (yellow dashed line) 1 sun illumination (green dashed dotted line) and in the dark (black circles). Arrows are drawn to clarify the trend with increasing light intensity.

Summary

Transient photocurrent and IS measurements were performed on hematite electrodes coated with varying thicknesses of Co-Pi catalyst. Transient photocurrent measurements showed that oxidation of Co(III) to Co(IV) is fast from valence band holes in hematite. This redox reaction is reversible and recombination of electrons from the conduction band to Co(IV) is also fast. An increasing $C_{Co\text{-}Pi}$ with

increasing thickness measured by IS showed that charge can be stored throughout the Co-Pi layer. Also, a decreasing $R_{ct,Co\text{-}Pi}$ with increasing Co-Pi thickness showed that the Co-Pi is porous and has catalytically active sites throughout. Despite efficient collection of photogenerated holes from the hematite electrode initial oxidation of the Co-Pi does not result in water oxidation at low applied potentials; instead it results in a charge separated state with the holes stored in the Co-Pi layer. Application of an additional potential is required to initiate water oxidation. One way of rationalizing this behavior is through a bimolecular water oxidation mechanism which requires the oxidation of 2 adjacent Co atoms before oxidizing water. This mechanism has been proposed for Co-Pi on FTO electrodes.[25] The requirement of 2 adjacent oxidized Co(IV) would correspond with some minimum Nernstian potential of the Co-Pi film or ratio between Co(III) and Co(IV). At more negative potentials, low band bending exists which causes a small amount of Co-Pi oxidation of Co(III) to Co(IV) from the valence band of hematite, and a large amount of recombination of Co(IV) to Co(III) from the conduction band of hematite, resulting in a relatively negative Nernstian potential of the Co-Pi film and no water oxidation. As a positive potential is applied, band bending is increased, oxidation of Co(III) to Co(IV) band is increased, recombination is decreased, the Nernstain potential of Co-Pi is shifted positive and water oxidation occurs. This concept is conceptualized in the relative energy diagram shown in figure 10.

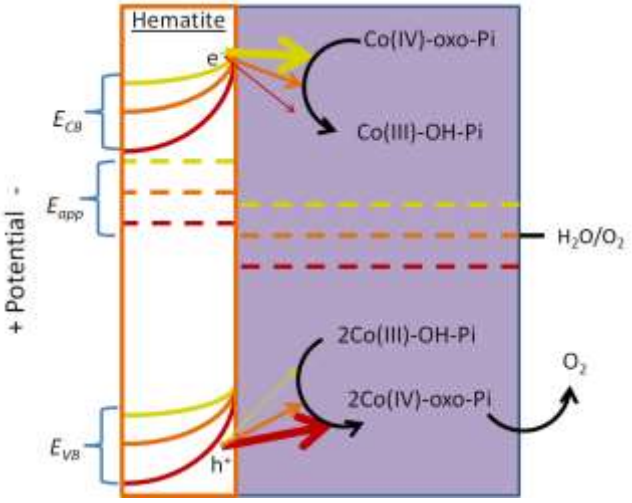

Figure 10. Relative energetics of a Co-Pi coated hematite electrode at under low(yellow), moderate (orange) and high (red) applied potentials.

Deposition of the Co-Pi catalyst to planar hematite electrodes produced a favorable shift in the photocurrent onset potential by ~200 to 250 mV. This shift increased with increasing Co-Pi thickness.

The framework described above is consistent with this result where it can be rationalized that increasing the Co-Pi thickness, separates charge better, reduces recombination and maintains a higher concentration of Co(IV) throughout the Co-Pi film for a given applied potential. The cathodic shifts measured in this study are higher than the ~180 mV shift observed when Co-Pi is deposited on hematite electrodes with higher surface area. [21-23] Also, for high surface area hematite, this value did not increase with Co-Pi thickness, and required the optimization of thin Co-Pi layers.[21,22] Based on the proposed framework, a higher surface area hematite electrode would provide a larger source of electrons to recombine with the Co(IV). Also, making thicker layers of Co-Pi on high surface area hematite is not necessarily correlated with better charge separation because of the three dimensional structure. Although the thin films used herein are not practical for achieving the highest photocurrents, the use of such films allowed us to perform a controlled thickness dependence which showed an increasing performance with increasing Co-Pi thickness; a trend consistent with Co-Pi on FTO.[25]

It was also found that at potentials >~1.4 V vs RHE, The photocurrent does not increase with increasing Co-Pi thickness. We propose that at these potentials, the Nernstian potential of the Co-Pi film is positive enough (there are enough adjacent Co(IV) active cites) that when a hole reaches the hematite-Co-Pi interface, it can be immediately turned into faradaic photocurrent (oxygen). This is consistent with current transients which instantaneously reach the maximum current upon illumination, as well as IS which shows the disappearance of the low frequency semicircle attributed to trapping of holes, be it in surface states for a bare electrode or in the Co-Pi for a Co-Pi coated electrode.[37,38] The slight increase in current with Co-Pi at positive potentials is attributed to the reduction in Fermi level pinning, indicated in the Mott Schottky plot.

Conclusion

It has been observed that several analogies can be drawn between the bare hematite electrode and the Co-Pi coated electrode. Both require the oxidation of a water oxidation active site to an intermediate before facile water oxidation occurs.[37,38] In the case of a bare electrode this is possibly the oxidation of an iron-hydroxide to an iron-oxo intermediate, although the identity of this iron-oxo intermediate has not yet been confirmed.[37,46,47] In the case of Co-Pi, this is likely the oxidation of a cobalt-hydroxyl to a cobalt-oxo intermediate (figure 10).[25,40] Both intermediates however, are subject to recombination or reduction by electrons in the conduction band. For both bare and Co-Pi coated electrodes, this recombination is turned off with an applied potential and high band bending. Co-Pi coated hematite electrodes differ from bare hematite electrodes by separating charge and reducing recombination.

Despite this improved charge separation, Co-Pi is not immune to recombination from electrons in the conduction band. For Co-Pi to improve photoanodes further, recombination of electrons from the conduction band must be reduced.

Acknowledgements

TWH thanks the National Science Foundation (CHE-1150378) for support of this research.

References

(1) Moomow, W.; Yamba, F.; Kamimoto, M.; Maurice, L.; Nyboer, J.; Urama, K.; Weir, T. In *IPCC Special Report on Renewable Energy Sources and Climate change Mitigation*; Edenhofer, O., Pichs-Madruga, R., Sokona, Y., Seyboth, K., Matschoss, P., Kadner, S., Zwickel, T., Eickemeier, P., Hansen, G., Schlömer, S., von Stechow, C., Eds.; Cambridge University Press: United Kingdom and New York, NY, USA, 2011.

(2) Lewis, N. S.; Nocera, D. G. *PNAS* **2006**, *103*, 15729.

(3) Fujishima, A.; Honda, K. *Nature* **1972**, *238*, 37.

(4) Kennedy, J. H.; Frese, K. W. *J. Electrochem. Soc.* **1978**, *125*, 709.

(5) Marusak, L. A.; Messier, R.; White, W. B. *J. Phys. Chem. Solids* **1980**, *41*, 981.

(6) Hardee, K. L.; Bard, A. J. *J. Electrochem. Soc.* **1977**, *124*, 215.

(7) Goodenough, J. B. *Progress in Solid State Chemistry* **1971**, *5*, 145.

(8) Kerisit, S.; Rosso, K. M. *The Journal of Chemical Physics* **2007**, *127*, 124706.

(9) Bjorksten, U.; Moser, J.; Gratzel, M. *Chem. Mat.* **1994**, *6*, 858.

(10) Kay, A.; Cesar, I.; Gratzel, M. *Journal of the American Chemical Society* **2006**, *128*, 15714.

(11) Duret, A.; Gratzel, M. *Journal of Physical Chemistry B* **2005**, *109*, 17184.

(12) Lin, Y. J.; Zhou, S.; Sheehan, S. W.; Wang, D. W. *Journal of the American Chemical Society* **2011**, *133*, 2398.

(13) Dareedwards, M. P.; Goodenough, J. B.; Hamnett, A.; Trevellick, P. R. *J. Chem. Soc., Faraday Trans. 1 F* **1983**, *79*, 2027.

(14) Upul Wijayantha, K. G.; Saremi-Yarahmadi, S.; Peter, L. M. *Physical Chemistry Chemical Physics* **2011**, *13*, 5264.

(15) Peter, L. M.; Wijayantha, K. G. U.; Tahir, A. A. *Faraday Discussions* **2012**, *155*, 309.

(16) Cowan, A. J.; Barnett, C. J.; Pendlebury, S. R.; Barroso, M.; Sivula, K.; Grätzel, M.; Durrant, J. R.; Klug, D. R. *Journal of the American Chemical Society* **2011**, *133*, 10134.

(17) Pendlebury, S. R.; Barroso, M.; Cowan, A. J.; Sivula, K.; Tang, J. W.; Gratzel, M.; Klug, D.; Durrant, J. R. *Chemical Communications* **2011**, *47*, 716.

(18) Tilley, S. D.; Cornuz, M.; Sivula, K.; Grätzel, M. *Angewandte Chemie International Edition* **2010**, *49*, 6405.

(19) McDonald, K. J.; Choi, K. S. *Chemistry of Materials* **2011**, *23*, 1686.

(20) Zhong, D. K.; Sun, J. W.; Inumaru, H.; Gamelin, D. R. *Journal of the American Chemical Society* **2009**, *131*, 6086.

(21) Zhong, D. K.; Gamelin, D. R. *Journal of the American Chemical Society* **2010**, *132*, 4202.

(22) Zhong, D. K.; Cornuz, M.; Sivula, K.; Graetzel, M.; Gamelin, D. R. *Energy & Environmental Science* **2011**, *4*, 1759.

(23) Barroso, M.; Cowan, A. J.; Pendlebury, S. R.; Grätzel, M.; Klug, D. R.; Durrant, J. R. *Journal of the American Chemical Society* **2011**, *133*, 14868.

(24) Cummings, C. Y.; Marken, F.; Peter, L. M.; Tahir, A. A.; Wijayantha, K. G. U. *Chemical Communications* **2012**.

(25) Surendranath, Y.; Kanan, M. W.; Nocera, D. G. *Journal of the American Chemical Society* **2010**, *132*, 16501.

(26) Kanan, M. W.; Nocera, D. G. *Science* **2008**, *321*, 1072.

(27) Lutterman, D. A.; Surendranath, Y.; Nocera, D. G. *Journal of the American Chemical Society* **2009**, *131*, 3838.

(28) Hong, Y.-R.; Liu, Z.; Al-Bukhari, S. F. B. S. A.; Lee, C. J. J.; Yung, D. L.; Chi, D.; Hor, T. S. A. *Chemical Communications* **2011**, *47*.

(29) Pilli, S. K.; Deutsch, T. G.; Furtak, T. E.; Turner, J. A.; Brown, L. D.; Herring, A. M. *Physical Chemistry Chemical Physics* **2012**, *14*, 7032.

(30) Abdi, F. F.; van de Krol, R. *The Journal of Physical Chemistry C* **2012**.

(31) Zhong, D. K.; Choi, S.; Gamelin, D. R. *Journal of the American Chemical Society* **2011**, *133*, 18370.

(32) Seabold, J. A.; Choi, K.-S. *Chemistry of Materials* **2011**, *23*, 1105.

(33) Steinmiller, E. M. P.; Choi, K.-S. *Proceedings of the National Academy of Sciences* **2009**, *106*, 20633.

(34) Martinson, A. B. F.; DeVries, M. J.; Libera, J. A.; Christensen, S. T.; Hupp, J. T.; Pellin, M. J.; Elam, J. W. *The Journal of Physical Chemistry C* **2011**, *115*, 4333.

(35) George, S. M. *Chem. Rev.* **2010**, *110*, 111.

(36) Klahr, B. M.; Martinson, A. B. F.; Hamann, T. W. *Langmuir* **2011**, *27*, 461.

(37) Klahr, B.; Giménez, S.; Fabregat-Santiago, F.; Hamann, T.; Bisquert, J. *Energy & Environmental Science* **2012**, *DOI: 10.1039/C2EE21414H*.

(38) Klahr, B.; Gimenez, S.; Fabregat-Santiago, F.; Hamann, T.; Bisquert, J. *Journal of the American Chemical Society* **2012**, *134*, 4294.

(39) Libera, J. A.; Hryn, J. N.; Elam, J. W. *Chemistry of Materials* **2011**, *23*, 2150.

(40) McAlpin, J. G.; Surendranath, Y.; Dincă, M.; Stich, T. A.; Stoian, S. A.; Casey, W. H.; Nocera, D. G.; Britt, R. D. *Journal of the American Chemical Society* **2010**, *132*, 6882.

(41) Symes, M. D.; Surendranath, Y.; Lutterman, D. A.; Nocera, D. G. *Journal of the American Chemical Society* **2011**, *133*, 5174.

(42) Sanchez, H. L.; Steinfink, H.; White, H. S. *Journal of Solid State Chemistry* **1982**, *41*, 90.

(43) Klahr, B. M.; Hamann, T. W. *Applied Physics Letters* **2011**, *99*, 3.

(44) Klahr, B. M.; Gimenez, S.; Fabregat-Santiago, F.; Hamann, T. W.; Bisquert, J. *Journal of the American Chemical Society* **2012**, *Forthcoming*.

(45) Klahr, B. M.; Hamann, T. W. *Journal of Physical Chemistry C* **2011**, *115*, 8393.

(46) Hellman, A.; Pala, R. G. S. *The Journal of Physical Chemistry C* **2011**, *115*, 12901.

(47) Trainor, T. P.; Chaka, A. M.; Eng, P. J.; Newville, M.; Waychunas, G. A.; Catalano, J. G.; Brown Jr, G. E. *Surface Science* **2004**, *573*, 204.